Time-dependent spin-density-functional-theory description of He^+-He collisions

Matthew Baxter* and Tom Kirchner†
Department of Physics and Astronomy, York University, Toronto, Ontario, Canada M3J 1P3

Eberhard Engel
Center for Scientific Computing, J. W. Goethe-Universität, D-60438 Frankfurt/Main, Germany
(Received 24 July 2017; published 12 September 2017)

Theoretical total cross-section results for all ionization and capture processes in the He^+-He collision system are presented in the approximate impact energy range of 10–1000 keV/amu. Calculations were performed within the framework of time-dependent spin-density functional theory. The Krieger-Li-Iafrate approximation was used to determine an accurate exchange-correlation potential in the exchange-only limit. The results of two models, one where electron translation factors in the orbitals used to calculate the potential are ignored and another where partial electron translation factors are included, are compared with available experimental data as well as a selection of previous theoretical calculations.

DOI: 10.1103/PhysRevA.96.032708

I. INTRODUCTION

The general ion-atom collision system carries active electrons on both the target and the projectile. A prototypical example from this class of problem is the He^+-He system which consists of a target with two electrons and a single electron on the projectile. A popular alternative is to consider an atomic hydrogen target (see, for example, Refs. [1,2]). However, in He^+-H collisions care must be taken when treating the distinct spin-singlet and triplet initial states [3].

A variety of charge transfer processes can occur in He^+-He collisions. The processes can be broadly categorized into those that involve one active electron,

$$He^+ + He \rightarrow He^+ + He^+ + e^-, \quad (1)$$

$$He^+ + He \rightarrow He + He^+, \quad (2)$$

$$He^+ + He \rightarrow He^{2+} + He + e^-, \quad (3)$$

those that involve two active electrons,

$$He^+ + He \rightarrow He^+ + He^{2+} + 2e^-, \quad (4)$$

$$He^+ + He \rightarrow He^{2+} + He^+ + 2e^-, \quad (5)$$

$$He^+ + He \rightarrow He + He^{2+} + e^-, \quad (6)$$

and those that involve three active electrons,

$$He^+ + He \rightarrow He^{2+} + He^{2+} + 3e^-. \quad (7)$$

Additionally there is the channel where no charges are transferred and the two channels that result in the production of He^-. Cross sections for the latter are known to be negligible [4,5].

Total cross sections for the processes described in Eqs. (1)–(7) have been calculated within a spin-density-functional-theory [6] framework, a generalization of time-dependent density functional theory (TDDFT) [7,8] to spin-dependent systems. The spin-polarized nature of the system accentuates the importance of exchange effects, which in turn necessitates an accurate exchange potential. An exploration of a procedure for calculating such a potential comprises the bulk of this work.

Experimental results for the various outcome channels over a large range of impact energies [9–17] provide a useful benchmark for this problem. Results can also be compared with the theoretical work of other groups. These calculations employ a variety of methods including classical models such as the over the barrier model [18], the Bohr-Lindhard model [19,20], and the classical trajectory Monte Carlo method [21]. Quantum mechanical calculations have been carried out using the local plasma approximation [22], the independent event model [23], and a plethora of perturbative calculations [24–30], the majority of which focus on single capture to the projectile [Eq. (2)]. A calculation that would address all physical outcome channels is still outstanding. One of the primary objectives of the present work is to fill this void.

We begin our discussion with an overview of some relevant aspects of time-dependent density functional theory in Sec. II A. This is followed by a description of the method used to calculate a time-dependent exchange potential in Sec. II B. This section also includes some details of the two-center basis generator method which was used to solve for the one-particle density. The theory section closes with a description of the final-state analysis for extracting the various outcome probabilities (Sec. II C). The results of our calculations are presented in Sec. III. Finally conclusions drawn from these studies are offered in Sec. IV.

Atomic units ($\hbar = m_e = e = 1$) are used unless stated otherwise.

II. THEORY

A. TDDFT

A system of N particles may be described by an N-particle wave function $\Psi(t)$ whose evolution is governed by the time-dependent Schrödinger equation (TDSE)

$$i\frac{\partial \Psi(t)}{\partial t} = \hat{H}(t)\Psi(t), \quad (8)$$

with a Hamiltonian $\hat{H}$ which may be written as

$$\hat{H}(t) = \hat{T} + \hat{V}_{ee} + \hat{V}_{\rm ext}(t), \quad (9)$$

*baxterma@yorku.ca
†tomk@yorku.ca

where $\hat{T}$ is the kinetic energy, $\hat{V}_{ee}$ are the two-particle interactions, and $\hat{V}_{\rm ext}$ is a time-dependent, one-particle interaction potential.

The computationally demanding two-body term $\hat{V}_{ee}$ makes direct solutions of the TDSE difficult. TDDFT [7,8] offers a solution to this problem. By making use of the one-to-one correspondence between the one-particle density

$$n(\mathbf{r}_1,t) = N \sum_{\sigma_1 \ldots \sigma_N} \int d^3r_2 \ldots d^3r_N \, |\Psi(\mathbf{x}_1, \ldots, \mathbf{x}_N, t)|^2 \quad (10)$$

and the external potential $\hat{V}_{\rm ext}$, where $x_i = (\mathbf{r}_i, \sigma_i)$ label the position and spin of the ith particle, guaranteed by the Runge-Gross theorem [6,31], the interacting system may be mapped onto a system of noninteracting particles.

This so-called Kohn-Sham (KS) system consists of N spin orbitals $\varphi_{j\sigma}$ which evolve according to the time-dependent KS equation

$$i\frac{\partial}{\partial t}\varphi_{j\sigma} = \left(-\frac{\Delta}{2} + v^{\sigma}_{\rm KS}[n_\uparrow, n_\downarrow](\mathbf{r},t)\right)\varphi_{j\sigma}(\mathbf{r},t), \quad (11)$$

such that

$$n(\mathbf{r},t) = \sum_{\sigma} \sum_{j=1}^{N_\sigma} |\varphi_{j\sigma}(\mathbf{r},t)|^2. \quad (12)$$

In Eq. (11) $n_\sigma, \sigma \in \{\uparrow, \downarrow\}$ are the spin-up and spin-down one-particle densities given by

$$n_\sigma = \sum_{j=1}^{N_\sigma} |\varphi_{j\sigma}|^2, \quad (13)$$

N_σ is the number of particles of a given spin projection σ, and $v^{\sigma}_{\rm KS}$ is the KS potential. The potential may be decomposed into several simpler objects:

$$v^{\sigma}_{\rm KS}[n_\uparrow, n_\downarrow] = v_{\rm ext} + v_{\rm H}[n] + v^{\sigma}_{\rm xc}[n_\uparrow, n_\downarrow]. \quad (14)$$

The first term in this expression is the external potential, which is the potential $\hat{V}_{\rm ext}$ of Eq. (9) on the single-particle level. For the He^+-He collision system considered in this work $v_{\rm ext}$ may be written, making use of the semiclassical approximation, as

$$v_{\rm ext}(\mathbf{r},t) = -\frac{2}{r} - \frac{2}{|\mathbf{r} - \mathbf{R}(t)|}, \quad (15)$$

where $\mathbf{R}(t) = (b, 0, Vt)$ is the straight-line trajectory of the projectile with velocity V and impact parameter (distance of closest approach) b.

The next term in Eq. (14) is the Hartree screening potential

$$v_{\rm H}(\mathbf{r},t) = \int \frac{n(\mathbf{r}',t)}{|\mathbf{r} - \mathbf{r}'|} d^3r', \quad (16)$$

which is an explicit functional of the full one-particle density. The last term is the exchange-correlation potential which encodes the complicated electron-electron interaction potential into the language of the noninteracting system. For convenience $v^{\sigma}_{\rm xc}$ is often further broken down into separate exchange and correlation potentials:

$$v^{\sigma}_{\rm xc} = v^{\sigma}_{\rm x} + v^{\sigma}_{\rm c}. \quad (17)$$

Splitting $v^{\sigma}_{\rm xc}$ into an exchange and correlation part facilitates the application of the x-only approximation where the correlation potential is taken to be zero ($v^{\sigma}_{\rm c} = 0$). Such a model which ignores dynamic correlation is usually referred to as an independent electron model (IEM). Within this approximation $v^{\sigma}_{\rm x}$ may be determined exactly via the optimized potential method (OPM) [32–34]. The complexity of the OPM makes it prohibitively difficult to implement in general. As a secondary option one may instead make use of the Krieger-Li-Iafrate approximation [35–37] (KLI). In many situations potentials generated using the KLI approximation are numerically close to those produced by the full OPM [38]. The success of the KLI approximation is due to the fact that it preserves several properties of the exact potential. In particular, the KLI approximation ensures the exact cancellation of the self-interaction in the Hartree term and thus maintains the correct asymptotics,

$$\lim_{r\to\infty} v^{\sigma}_{\rm x}(\mathbf{r}) = -\frac{1}{r}. \quad (18)$$

B. The exchange potential

The one-particle density was determined by solving Eq. (11) using the two-center basis generator method [39] (TC-BGM). As mentioned above this relies upon the specification of an exchange-correlation potential. While the correlation potential may be ignored, that is, the x-only approximation may be used (with some understanding of the consequences), an accurate exchange potential is essential for a precise description of the He^+-He collision system. The spin-polarized nature of the system, which emphasizes exchange effects, makes this fact indisputable. To this end the KLI approximation to the OPM was employed in the calculation of $v^{\sigma}_{\rm x}$.

The ground-state density functional theory (DFT) scheme of Ref. [40] has been adapted to calculate a time-dependent exchange potential. At any instant of time, t, the He^+-He system may be regarded as a diatomic quasimolecule with an internuclear distance $R(t) = \sqrt{b^2 + Z(t)^2}$, where b is the impact parameter and Z is the position of the projectile as described below Eq. (15). If at each time step of the TC-BGM the time-dependent KS orbitals $\varphi_{\sigma j}(\mathbf{r},t)$ are fed into the KLI functional, a time-dependent exchange potential, $v^{\sigma}_{\rm x}[\{\varphi_{\sigma j}\}; t]$, is obtained:[1]

$$v^{{\rm KLI},\sigma}_{\rm x}(\mathbf{r},t) = \frac{1}{2n_\sigma(\mathbf{r},t)} \sum_{j=1}^{N_\sigma} \Big\{ \left[e^{\sigma}_{{\rm x},j}(\mathbf{r},t) + {\rm c.c.}\right] + |\varphi_{j\sigma}(\mathbf{r},t)|^2 \Delta_{j\sigma}(t) \Big\}, \quad (20)$$

$$\Delta_{j\sigma}(t) = \int d^3r \left\{ |\varphi_{j\sigma}(\mathbf{r},t)|^2 v^{{\rm KLI},\sigma}_{\rm x}(\mathbf{r},t) - e^{\sigma}_{{\rm x},j}(\mathbf{r},t) \right\} + {\rm c.c.}, \quad (21)$$

[1]The normalization of the KLI potential is chosen so that

$$v^{\rm KLI}_{\rm x}(\mathbf{r},t) \xrightarrow{|\mathbf{r}|\to\infty} 0. \quad (19)$$

$$e^{\sigma}_{\mathrm{x},j}(\mathbf{r},t) = -\sum_{k=1}^{N_\sigma} \varphi^*_{j\sigma}(\mathbf{r},t)\varphi_{k\sigma}(\mathbf{r},t) \times \int d^3r' \, \frac{\varphi^*_{k\sigma}(\mathbf{r}',t)\,\varphi_{j\sigma}(\mathbf{r}',t)}{|\mathbf{r}-\mathbf{r}'|}. \tag{22}$$

In Ref. [40] the KLI scheme has been implemented for eigenstates of a total KS potential which is invariant against rotation around the internuclear axis. This restriction complicates the use of the corresponding KLI potential, since the present $\varphi_{j\sigma}$ orbitals do not exhibit any specific symmetry.

In order to detail a solution to the symmetry problem a more thorough description of the TC-BGM is necessary. Within the TC-BGM the KS orbitals are represented in a nonorthogonal basis,

$$\varphi_{\sigma j}(\mathbf{r},t) = \sum_{c\in\{P,T\}} \sum_{k,L} d^{\sigma j}_{ckL}(t)\tilde{\chi}^L_{ck}(\mathbf{r},t), \tag{23}$$

where

$$\tilde{\chi}^L_{ck}(\mathbf{r},t) = \begin{cases} e^{i\mathbf{v}_T\cdot\mathbf{r}}\chi^L_{ck}(\mathbf{r},t), & c = T, \\ e^{i\mathbf{v}_P\cdot\mathbf{r}}\chi^L_{ck}(\mathbf{r},t), & c = P, \end{cases} \tag{24}$$

which are the basis functions with electron translation factors (ETFs) included. The basis functions themselves are given by

$$\chi^L_{ck}(\mathbf{r},t) = W_P(\mathbf{r},t,\epsilon_P)^L\chi^0_{ck}(\mathbf{r}), \tag{25}$$

with

$$W_P(\mathbf{r},t,\epsilon_P) = \frac{1-e^{-\epsilon_P|\mathbf{r}_T-\mathbf{R}(t)|}}{|\mathbf{r}_T-\mathbf{R}(t)|}, \tag{26}$$

where $\mathbf{r}_T$ represents the position vector with respect to the target center.

In Eq. (25) the functions χ^0_{ck} are the bound orbitals for the target helium atom ($c = T$) and the projectile helium ion ($c = P$). Additional states generated by a target potential operator are possible (see, for example, Ref. [41]). However, in order to keep the number of states in the basis to a minimum and simplify the description only the pseudostates generated with W_P are included. This simplification has proven sufficient in the past [42]. The remaining regularizer is set to $\epsilon_P = 1$. The complete basis set used may be described in terms of the maximum L value included for each bound subshell, $1s$–$4f$, indexed by k, in the basis. These values are listed in Table I and total 124 basis states.

It is clear from the above description that only the basis states corresponding to s-type orbitals will make cylindrically symmetric contributions to the KS orbitals. The simplest solution is to only feed the $1s$ contributions into the KLI functional. While higher s states are also admissible they will no longer represent the most occupied subshell, meaning their inclusion will do little to improve the accuracy of the description of a given orbital. Leaving out ETFs for the time being the orbitals will take the explicit form

$$\varphi^{1s}_{\sigma j}(\mathbf{r},t) = a^{\sigma j}_T(t)\chi^0_{T1}(\mathbf{r},t) + a^{\sigma j}_P(t)\chi^0_{P1}(\mathbf{r},t). \tag{27}$$

The coefficients are the result of projecting the KS orbitals onto the two-dimensional subspace spanned by the target and the projectile $1s$ states

$$|\varphi^{1s}_{\sigma j}\rangle = \hat{P}\,|\varphi_{\sigma j}\rangle = \sum_{c_1,c_2\in\{T,P\}} \tilde{S}^{-1}_{c_1c_2}|\chi^0_{c_1 1}\rangle\langle\chi^0_{c_2 1}|\varphi_{\sigma j}\rangle, \tag{28}$$

with $\tilde{S}^{-1}_{c_1c_2}$ being the inverse of the overlap matrix

$$\tilde{S}_{c_1c_2} = \langle\chi^0_{c_1 1}|\chi^0_{c_2 1}\rangle. \tag{29}$$

The coefficients are then determined to be

$$a^{\sigma j}_c = \sum_{c_1,c_2\in\{T,P\}} \sum_{k=1}^{K}\sum_{l=0}^{L} \tilde{S}^{-1}_{cc_1} S^{c_2\,k\,l}_{c\,1\,0}\, d^{\sigma j}_{c_2 kl}, \tag{30}$$

with

$$S^{c_2\,k_2\,l_2}_{c_1\,k_1\,l_1} = \langle\chi^{l_1}_{c_1k_1}|\chi^{l_2}_{c_2k_2}\rangle \tag{31}$$

being the full overlap matrix.

Returning to the question of the ETFs, working in the rotating center-of-mass frame in which the z direction points along the internuclear axis the ETFs become

$$e^{i\mathbf{v}_T\cdot\mathbf{r}} = e^{\frac{iV}{2}(x\sin\theta - z\cos\theta)}, \tag{32a}$$

$$e^{i\mathbf{v}_P\cdot\mathbf{r}} = e^{\frac{iV}{2}(z\cos\theta - x\sin\theta)}, \tag{32b}$$

where $\theta = \arctan b/Z$ and V is the relative velocity of the centers, the same velocity appearing below Eq. (15). If we now introduce a two-centered coordinate system, placing the foci at the two nuclear centers

$$\begin{aligned} x &= \frac{|R|}{2}\sqrt{(\xi^2-1)(1-\eta^2)}\sin\phi, \\ y &= \frac{|R|}{2}\sqrt{(\xi^2-1)(1-\eta^2)}\cos\phi, \\ z &= \frac{|R|}{2}\xi\eta, \end{aligned} \tag{33}$$

it becomes clear that the portion of the ETFs containing x violates the desired cylindrical symmetry.

Two obvious solutions present themselves. First, one may simply ignore the ETFs completely. This would amount to passing the orbitals described by Eq. (27) into the KLI functional. Alternatively the symmetry-breaking portions of the ETFs may be dropped. In this case the full $1s$-only KS orbital becomes

$$\tilde{\varphi}^{1s}_{\sigma j}(\mathbf{r},t) = a^{\sigma j}_T(t)e^{-\frac{iVz\cos\theta}{2}}\chi^0_{T1}(\mathbf{r},t) + a^{\sigma j}_P(t)e^{\frac{iVz\cos\theta}{2}}\chi^0_{P1}(\mathbf{r},t). \tag{34}$$

This will offer at least some of the correction provided by the full ETF. Unfortunately, as the internuclear coordinate $Z(t)$ approaches 0 (corresponding to $\theta = \frac{\pi}{2}$) the partial ETF will tend to 1, meaning that when the target and the projectile are at their closest, the most active region of the collision, no ETF will be present.

TABLE I. Description of the TC-BGM basis expansion.

State	$1s$	$2s$	$2p$	$3s$	$3p$	$3d$	$4s$	$4p$	$4d$	$4f$
k	1	2	3, 4	5	6, 7	8–10	11	12, 13	14–16	17–20
$L_{\max}$	0	0	1	1	2	2	2	3	3	3

Regardless of which option is chosen it is important that v_H be determined with the same set of orbitals used in the calculation of v_x^σ, preserving the precise cancellation of the self-interaction present in the Hartree potential.

C. Final-state analysis

Of interest in any scattering problem is the probability of finding the system in some final state. If we represent the state being considered as $|f_1\ f_2\ f_3\rangle$ and the initial state of the system propagated to some final time t_f by $|\varphi_{\uparrow 1}\,\varphi_{\uparrow 2}\,\varphi_{\downarrow 1}(t_f)\rangle$, the exclusive probability to find the system in the given final state at time t_f will be given by

$$P_{f_1 f_2 f_3}(t_f) = |\langle f_1\ f_2\ f_3|\varphi_{\uparrow 1}\,\varphi_{\uparrow 2}\,\varphi_{\downarrow 1}(t_f)\rangle|^2. \tag{35}$$

If one assumes that both the propagated and the final states can be represented as sinlge Slater determinants then the probability in question may be expressed in the form

$$P_{f_1 f_2 f_3}(t_f) = \det[\gamma_{ff'}(t_f)], \tag{36}$$

where $\gamma_{ff'}$ is the one-particle density matrix

$$\gamma_{ff'}(t_f) = \sum_\sigma \sum_{j=1}^{N_\sigma} \langle f|\varphi_{\sigma j}(t_f)\rangle\,\langle\varphi_{\sigma j}(t_f)|f'\rangle\,, \tag{37}$$

with f and $f' \in \{f_1, f_2, f_3\}$, and the transition amplitudes $\langle f|\varphi_{\sigma j}(t_f)\rangle = \langle\tilde{\chi}^l_{ck}|\varphi_{\sigma j}(t_f)\rangle$ (for some k, l, c, and properly orthogonalized basis functions $\tilde{\chi}^l_{ck}$) readily calculable from the dynamics. A model of this type which ignores the functional correlations [43] is consistent with an IEM description.

Alternatively, one could consider the probability to explicitly measure the states of some subset of the total number of particles. These so-called inclusive probabilities can be expressed in terms of determinants of submatrices of the density matrix [44].

In the current problem we are interested in those probabilities which correspond to the outcome channels of Eqs. (1)–(7). In such configurations we find k particles on the projectile, l particles in the continuum, and $3-k-l$ on the target ($0 \leqslant k \leqslant 3$ and $0 \leqslant l \leqslant 3-k$). The probabilities p_{kl} may be calculated in terms of sums of inclusive probabilities to find a given number of particles in the bound states of the target and the projectile by applying the machinery of Ref. [44] (see, for example, Refs. [45–47]). With the probabilities in hand the corresponding total cross section for each channel may then be calculated from (if we ignore σ_{10} which includes the elastic channel and must be treated with more care)

$$\sigma_{kl} = 2\pi \int_0^\infty b p_{kl}(b) db. \tag{38}$$

III. DISCUSSION

In what follows all results obtained by propagating the full KS orbitals in a potential generated from the $1s$-only orbitals of Eq. (27) that include no electron translation factors are designated by nETF. Those obtained by an application of the same processes using the $1s$-only orbitals, with partial ETFs, of Eq. (34) are referred to as pETF.

Before discussing the total cross section results we present some of the lower level features of the calculations. We consider the single-particle probabilities for each electron to ionize and to switch the nuclear center to which it is bound. These probabilities can be calculated from the transition amplitudes. As an example, if $\varphi_{\uparrow 1}$ begins initially on the target then the single-particle probability to ionize this electron can be written as

$$p(\mathrm{He}(\uparrow_1) \to I) = \sum_{c\in\{T,P\}} \sum_{k=1}^{K} \sum_{l=1}^{L} \left|\langle\tilde{\chi}^l_{ck}|\varphi_{\uparrow 1}(t_f)\rangle\right|^2 \tag{39}$$

and the single-particle probability to transfer to the projectile may be written as

$$p[\mathrm{He}(\uparrow_1) \to \mathrm{He}^+] = \sum_{k=1}^{K} \left|\langle\tilde{\chi}^1_{Pk}|\varphi_{\uparrow 1}(t_f)\rangle\right|^2, \tag{40}$$

where the probabilities are defined in terms of orthogonalized orbitals including full ETFs. These probabilities are presented for the pETF model for an impact energy ($E_P = \frac{1}{2} m_{\mathrm{He}} V^2$) of 40 keV/amu in Fig. 1. At this impact energy capture is the the dominant process. As one would expect, the probability to ionize the more tightly bound He^+ electron is consistently less than that for either of the He electrons. Also of note is the obvious difference between the two He electrons, a clear reflection of the implementation of a spin-dependent potential.

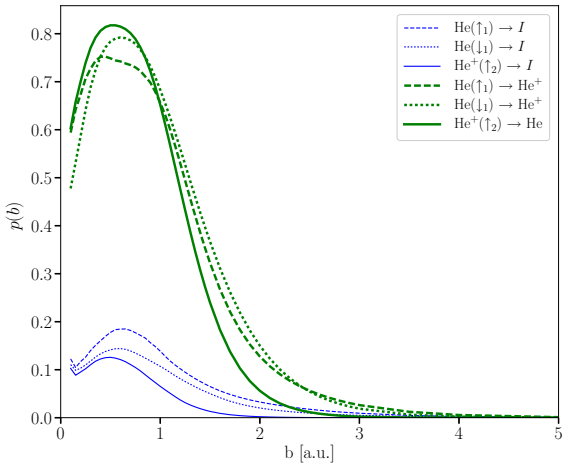

FIG. 1. Single-particle probabilities for each spin orbital to transfer between centers (thick lines) and to ionize (thin lines) in the pETF model for an impact energy of 40 keV/amu.

Total cross sections for the processes described in Eqs. (1)–(7) are presented in Figs. 2–8. Where available the results of the current work are compared with calculations of other groups. It should be noted that only those calculations that describe the system quantum mechanically were considered, that is to say, works that employ approaches such as the classical trajectory Monte Carlo method are not included.

We begin the discussion by considering the single target ionization process of Eq. (1). The results for this channel, σ_{11}, are presented in Fig. 2. Both nETF and pETF are in good agreement with experiment throughout the full range of impact energies. As the impact energy increases a slight gap opens between the two. This trend is, as one would expect, due to the fact that ETFs should become more relevant as the relative velocity between the target and the projectile increases. The

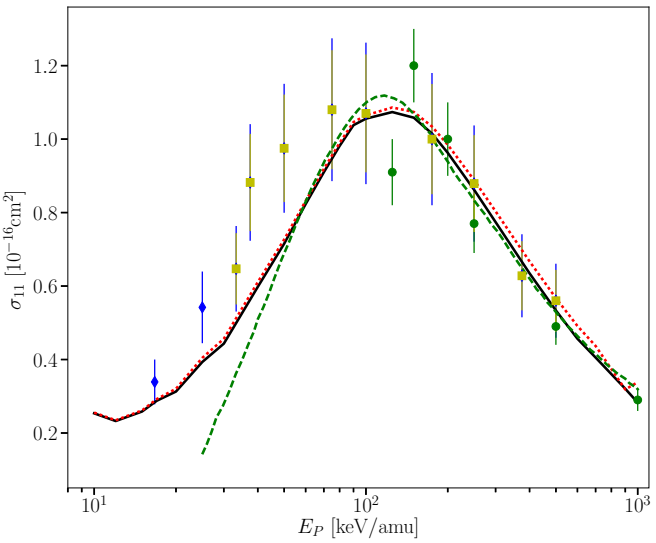

FIG. 2. Total cross section for single ionization of the target. Theoretical results: pETF (solid line), nETF (dotted line), and CDW-EIS of Miraglia and Gravielle [27] (dashed line). Experimental data: Diamonds [14], circles [16], and squares [13].

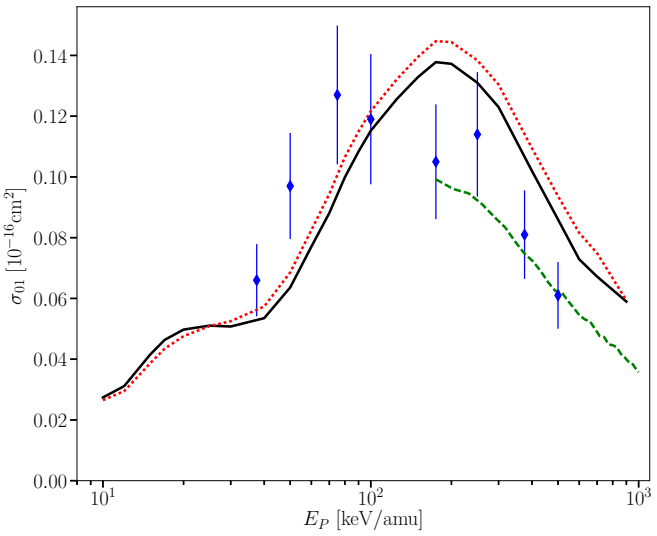

FIG. 3. Total cross section for single ionization of the projectile. Theoretical results: pETF (solid line), nETF (dotted line), and IEVM of Sigaud and Montenegro [23] (dashed line). Experimental data: Diamonds [14].

slightly lower values for the pETF version above 200 keV/amu make it a better fit to experiment. The underestimation of both curves below the peak corresponds almost exactly with the region where σ_{20} results begin to rise above the experimental results (see Fig. 4).

Also displayed in Fig. 2 are the continuum-distorted-wave eikonal-initial-state approximation (CDW-EIS) results of Miraglia and Gravielle [27]. These results seem to compliment the results of the present work through the majority of the impact energy range. One notable exception to this is the slightly higher cross-section maximum however. As there is a fairly large spread in the experimental data around this region it is difficult to say which is more accurate. The results of Miraglia and Gravielle [27] also begin to diverge as one approaches lower impact energies. This feature is likely due in large part to the perturbative nature of the CDW-EIS which becomes less reliable as one decreases the impact energy.

Next, we consider the results for σ_{01} [Eq. (3)] shown in Fig. 3. As with the previous channel both nETF and pETF results are in reasonable agreement with the experiment where it is available. Also continuing the trend seen in the σ_{11} results, both models begin essentially equal at low impact energies and separate as E_P increases. Both models begin to overestimate the data above the peak around 200 keV/amu. Once again the slightly lower pETF results are in better agreement with experiment. The slight unphysical structures in the curves below 40 keV/amu seem to correspond with the peaks of the σ_{00} channel (not pictured here). This issue is discussed in greater detail below.

These calculations have been compared with the independent event model (IEVM) results of Sigaud and Montenegro [23]. While the authors do not directly report σ_{01} they do present σ_{02}, σ_{03}, and what they call total electron loss (we denote this by σ_{total}). Using the relation

$$\sigma_{\text{total}} = \sigma_{01} + \sigma_{02} + \sigma_{03} \tag{41}$$

one can easily determine σ_{01} from their disclosed results. Their values seem to be in much better agreement with experiment in the high-energy range than either the nETF model or the pETF model. This can perhaps be explained by the presence of correlation in the IEVM calculations. As is discussed in more detail below, both of our models underestimate σ_{02} and σ_{03} in this impact energy range. Keeping in mind that $\sum p_{kl} = 1$ the increase in these channels resulting from the incorporation of correlation effects, so-called antiscreening in particular, would be drawn in part from the current channel of focus σ_{01} resulting in a decrease, putting our results in better agreement with both the results of Sigaud and Montenegro [23] and the experimental data.

For the results of single electron capture to the projectile, the process of Eq. (2) depicted in Fig. 4, both nETF and pETF models are essentially identical. This is what one would hope for as they are in good agreement with experiment in the entire range of impact energies. A possible explanation of the slight discrepancy between theory and experiment in the 50–150 keV/amu interval is offered by a comparison with the four-body Coulomb-Born distorted-wave approximation (CDBW-4B) results of Ghanbari-Adivi and Ghavaminia [30]. The correlation effects included in this model may point to the slight rise in cross section being related to the fact that we have employed an IEM approximation. Alternatively, the rise may be due to a failure of the partial ETF.

The latter explanation may provide a more satisfying solution to this problem. One would expect that capture processes should be dominated by the contributions of slow and close collisions. The region where the nETF and pETF models start to diverge from experiment is approximately the region where both models begin to diverge in other channels [see, for example, σ_{12} in Fig. 5], that is, the lowest energies where ETFs are important. Additionally they begin to agree with experiment once the cross sections begin to rapidly approach 0, for fast collisions. This would seem to

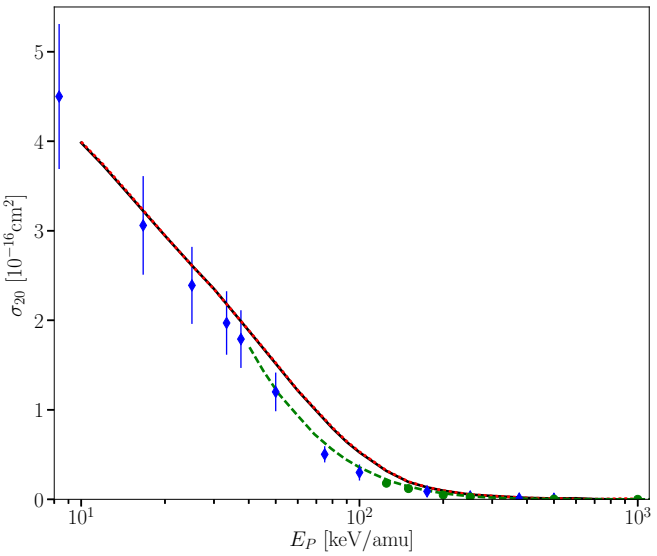

FIG. 4. Total cross section for single capture to the projectile. Theoretical results: pETF (solid line), nETF (dotted line), and CDBW-4B (post form) of Ghanbari-Adivi and Ghavaminia [30] (dashed line). Experimental data: Diamonds [14] and circles [16].

be an indication that correct ETFs are important for capture processes (a fact that should be at least intuitively obvious).

A few words should be spent addressing the choice of the theoretical calculation to be compared against. Unlike other channels there exists a relatively large number of works to select from that fit the criteria listed above. As the majority of these belong to a family of related perturbative models [24–30], the latest, that of Ghanbari-Adivi and Ghavaminia, was chosen. A comparison of the work of Ghanbari-Adivi and Ghavaminia with several earlier perturbative calculations can be found in Ref. [30].

With the single-electron processes taken care of, double target ionization, Eq. (4), the first of the two-electron processes

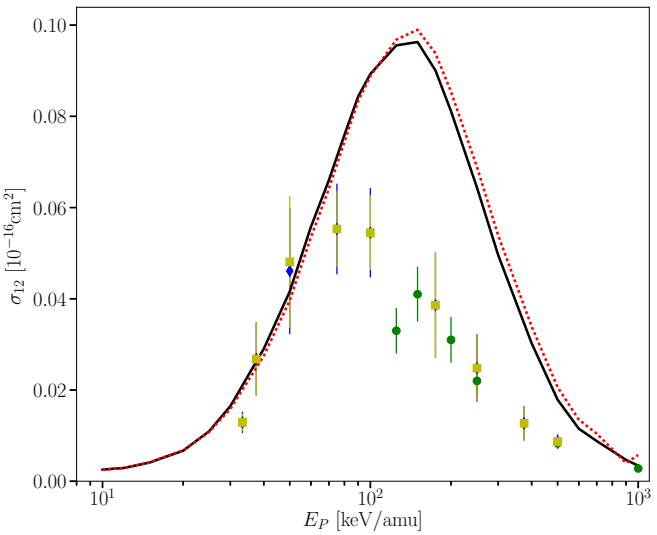

FIG. 5. Total cross section for double ionization of the target. Theoretical results: pETF (solid line) and nETF (dotted line). Experimental data: Diamonds [14], circles [16], and squares [13].

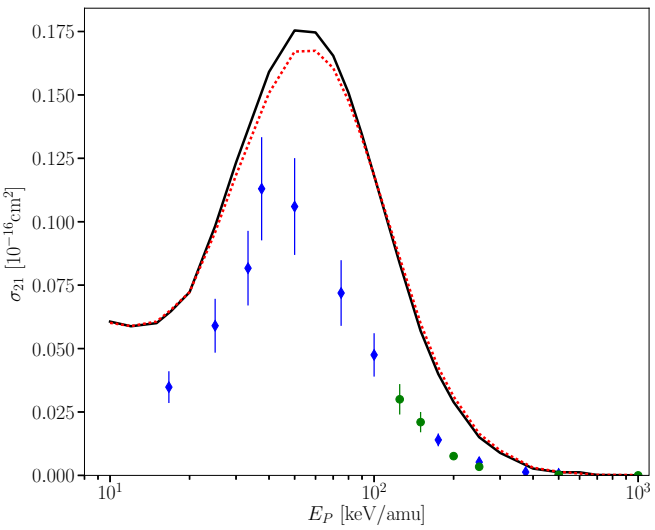

FIG. 6. Total cross section for transfer ionization of the target. Theoretical results: pETF (solid line) and nETF (dotted line). Experimental data: Diamonds [14] and circles [16].

is considered next. The results for this channel are presented in Fig. 5. As with previous channels both nETF and pETF results appear to be very similar, with a slight edge going to the pETF model's marginally lower results above 100 keV/amu. Both models seem to shift the peak in the cross section to higher impact energy than experiment would suggest is correct. As one would expect from an IEM the two models exaggerate double ionization (see, for example, Refs. [43,48]). As there are no previous works fitting the conditions for inclusion listed earlier, little else can be concluded about the results of the present work.

Another channel where the literature lacks a proper touchstone is that of transfer ionization [Eq. (6) shown in Fig. 6]. The trends for σ_{21} are very similar to those for σ_{12}. As with the previously discussed process both models are above experiment and shift the experimental peak to a higher impact energy. The only significant difference is that this is one of the few channels where the nETF model tends to give smaller cross section values and is in slightly better agreement with experiment than the pETF. The flattening of the curves below 20 keV/amu is an artifact of the TC-BGM becoming less reliable at the lowest impact energies.

The last two-electron process is simultaneous single ionization of the target and the projectile, Eq. (5). The results for our nETF and pETF models are presented in Fig. 7. These results both follow the trend of the data quite closely, arguably matching the position of the peak in the experimental cross sections. This channel is the second of two where the nETF model has a slight edge over the results of the pETF model. Unfortunately they fall below experiment for the majority of the impact energy range shown.

A comparison with the IEVM of Sigaud and Montenegro [23] explains this fact. Sigaud and Montenegro claim to capture the effects of antiscreening, the direct interaction between target and projectile electrons, which becomes increasingly important for projectile ionization processes at larger impact energies. As the results of the current work are those of an independent electron model (IEM) they make no effort

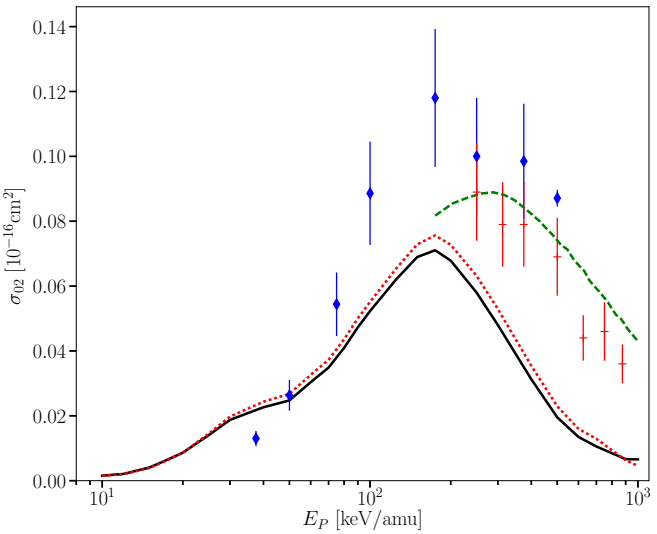

FIG. 7. Total cross section for simultaneous single ionization of the target and the projectile. Theoretical results: pETF (solid line), nETF (dotted line), and IEVM of Sigaud and Montenegro [23] (dashed line). Experimental data: Diamonds [14] and crosses [17].

to capture any correlation effects. Sigaud and Montenegro's efforts to capture antiscreening see their results fall within experiment for their entire extent. Encouragingly, if one were to extend the curve of Sigaud and Montenegro it would seem to overlap with the results of the present work, lending credence to the curve in the region below the cross section peak, where antiscreening cannot contribute.

Finally we consider the sole three-electron process, simultaneous double target and single projectile ionization [Eq. (7)]. The results, presented in Fig. 8, again follow the general trends found in the previously discussed channels: overestimation of the cross section peak and a slightly better showing for the pETF model over the results of the nETF model. Unlike for previous channels our results are in better agreement

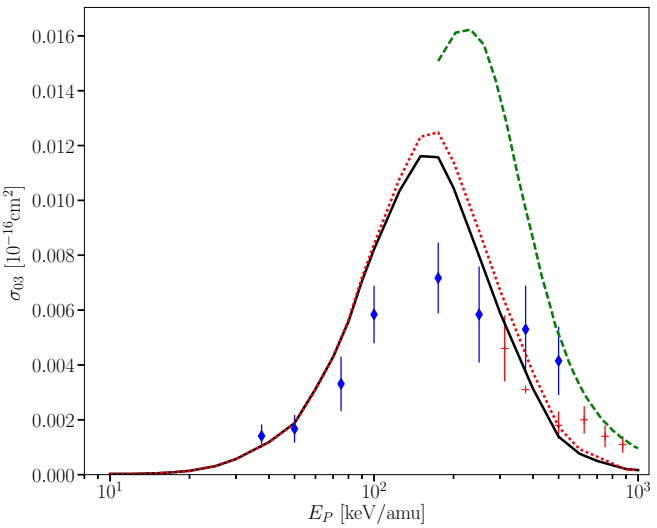

FIG. 8. Total cross section for simultaneous double target and single projectile ionization. Theoretical results: pETF (solid line), nETF (dotted line), and IEVM of Sigaud and Montenegro [23] (dashed line). Experimental data: Diamonds [14] and crosses [17].

with experiment than those of Sigaud and Montenegro [23], which overestimate the cross sections to a greater extent and over a larger impact energy range. As in previous channels the underestimation of our cross sections at larger impact energies may be attributed to correlation effects, in particular, to antiscreening which Sigaud and Montenegro [23] seem to exaggerate in this channel.

In addition to the outcome channels discussed above there are three further processes. One, σ_{10}, has been left out as it involves no charge transfer. The other two, σ_{00} and σ_{30}, involve all three electrons bound to either the target or the projectile. As is pointed out in the Introduction, these channels should not be considered due to the fact that the production cross sections for these configurations should be negligible. While modeling the initial and final states of the system as single Slater determinants accounts for Pauli exclusion which precludes all three electrons from occupying the ground state, there is nothing in the model to stop additional electrons from capturing and remaining in excited states. The only recourse, short of implementing a model which contains at least some functional correlation, is to artificially redistribute the probability from p_{00} and p_{30} into other channels.

Two options immediately present themselves. The first possibility is to feed the extra probability into the corresponding ionization channels. In other words, p_{00} and p_{30} would augment p_{01} and p_{21}, respectively. With the peak in σ_{30} approximately matching that of σ_{21} in both position and magnitude this solution would lead to a doubling of the overestimation present in the σ_{21} channel. A similar issue would arise in the lower impact energy range of the σ_{01} curve. This leaves one with the second option, to put the extra probability from p_{00} into p_{10} and feed p_{30} into p_{20}. The only effect this could have on the presented results would be to increase σ_{20}; however, as σ_{30} is at worst an order of magnitude less than σ_{20}, it would provide only a small shift in the curve displayed in Fig. 4.

One last point must be mentioned before closing this discussion. Above 500 keV/amu several of the cross-section curves exhibit minor spurious structures. These are the result of numerical issues that, above this impact energy, limit the minimum possible impact parameter for which the calculations produce results from 0.1 a.u. below 500 keV/amu gradually to 0.8 a.u. at 1000 keV/amu. In Eq. (38) the integrand, $b\,p(b)$, is approximated by a cubic spline which is, in turn, integrated to arrive at a cross section. The structure of the integrand means that so long as $p(0)$ is finite its value is irrelevant and we always know the integrand at $b = 0$. In the best-possible scenario the lower bound on the error of a cubic spline will scale to the fourth power in the largest step between knots [49]. The step size factor in the error bound then increases from 0.0001 to 0.4096, an increase by an approximate factor of 4000. It is this decrease in the accuracy of the interpolation which results in the minor structures above 500 keV/amu. The presence of these unphysical structures is the reason for the lack of a data point at 1000 keV/amu in Fig. 3.

IV. CONCLUSIONS

In this work we have presented an investigation of the He^+-He collision system within time-dependent spin-density

functional theory under the constraints of the exchange-only approximation. An accurate time-dependent exchange potential was determined through the application of the KLI approximation. Total cross-section results for all physical outcome channels were then offered in the approximate impact energy of range 10–1000 keV/amu for two models: one in which electron translation factors in the calculation of the potential were ignored and a second model where partial ETFs were used. The results of both models are in overall good agreement with experiment. Additionally, the current work is the only quantum-mechanical approach which captures all outcome channels over such a wide range of impact energies.

Without diminishing the results of this work it is necessary to highlight a few limitations and where the results may be improved in future iterations. First, the restriction of the implementation of the KLI functional to systems of cylindrical symmetry is the impetus for both the $1s$-only approximation as well as the need to consider both the nETF and the pETF models. Future applications of the procedure laid out in this work would benefit greatly from a fully three-dimensional implementation of the KLI functional that makes no symmetry assumptions.

Comparisons of our results with the theoretical works of other groups point to the fact that the calculations would also gain from the inclusion of correlation effects. Treating this x-only version as a proof of concept, there is nothing, apart from the added complexity of the calculations, precluding the addition of dynamic correlation through the application of any number of ground-state correlation functionals in the future. It should be noted that such a model would still not offer a complete description of time-dependent correlation; it would, for example, lack memory effects [7]. An added difficulty would be the inclusion of functional correlation effects. In order to move beyond the IEM single Slater determinant description of outcome probabilities, one would have to adapt a model similar to that of Wilken and Bauer [50] used in Ref. [43] to explicitly spin-polarized systems.

ACKNOWLEDGMENTS

This work was supported by the Natural Sciences and Engineering Research Council of Canada (NSERC) under Grant No. RGPIN-2014-03611. Additionally, this work was made possible by the facilities of the Shared Hierarchical Academic Research Computing Network (SHARCNET) and Compute/Calcul Canada. M.B. acknowledges the financial support provided by the Ontario Graduate and Queen Elizabeth II scholarships which are jointly funded by the province of Ontario and York University (Canada).

[1] J. Kuang, Z. Chen, and C. D. Lin, Excitation and charge transfer in $He^+ + H$ collisions, J. Phys. B **28**, 2173 (1995).

[2] L. F. Errea, L. Mendez, and A. Riera, Comment on 'formation of $H(2p)$ and $H(2s)$ in collisions of He^+ with H atoms', J. Phys. B **28**, 907 (1995).

[3] J. B. Wang, J. P. Hansen, and A. Dubois, Spin Anisotropy for Excitation in Collisions Between Two One-Electron Atoms, Phys. Rev. Lett. **85**, 1638 (2000).

[4] R. E. Miers, A. S. Schlachter, and L. W. Anderson, Production and loss of fast metastable helium atoms in collisions with Xe, H_2, Ar, and He, Phys. Rev. **183**, 213 (1969).

[5] S. K. Allison, Experimental results on charge-changing collisions of hydrogen and helium atoms and ions at kinetic energies above 0.2 keV, Rev. Mod. Phys. **30**, 1137 (1958).

[6] M. Petersilka and E. K. U. Gross, Spin-multiplet energies from time-dependent density functional theory, Int. J. Quantum Chem. **60**, 1393 (1996).

[7] *Fundamentals of Time-Dependent Density Functional Theory*, edited by Miguel A. L. Marques *et al.*, Lecture Notes in Physics Vol. 837 (Springer, Berlin, 2012).

[8] C. A. Ullrich, *Time-Dependent Density-Functional Theory: Concepts and Applications* (Oxford Scholarship Online, 2013).

[9] C. F. Barnett and P. M. Stier, Charge exchange cross sections for helium ions in gases, Phys. Rev. **109**, 385 (1958).

[10] E. A. Hinds and R. Novick, Precise resonant charge-transfer cross sections for He-He^+ between 2 and 100 eV, J. Phys. B **11**, 2201 (1978).

[11] R. Hegerberg, T. Stefansson, and M. T. Elford, Measurement of the symmetric charge-exchange cross section in helium and argon in the impact energy range 1–10 keV, J. Phys. B **11**, 133 (1978).

[12] N. V. de Castro Faria, F. L. Freire, and A. G. de Pinho, Electron loss and capture by fast helium ions in noble gases, Phys. Rev. A **37**, 280 (1988).

[13] R. D. DuBois and L. H. Toburen, Single and double ionization of helium by neutral-particle to fully stripped ion impact, Phys. Rev. A **38**, 3960 (1988).

[14] R. D. DuBois, Multiple ionization in He^+–rare-gas collisions, Phys. Rev. A **39**, 4440 (1989).

[15] H. Atan, W. Steckelmacher, and M. W. Lucas, Single electron loss and single electron capture for 0.6–2.2 MeV He^+ colliding with rare gases, J. Phys. B **24**, 2559 (1991).

[16] J. L. Forest, J. A. Tanis, S. M. Ferguson, R. R. Haar, K. Lifrieri, and V. L. Plano, Single and double ionization of helium by intermediate-to-high-velocity He^+ projectiles, Phys. Rev. A **52**, 350 (1995).

[17] A. C. F. Santos, G. M. Sigaud, W. S. Melo, M. M. Sant'Anna, and E. C. Montenegro, Absolute cross sections for projectile electron loss accompanied by target multiple ionization in collisions of He^+ with noble gases, J. Phys. B **44**, 045202 (2011).

[18] L. Chen and X. Chen, One and two electron transitions in multiply charged ions and helium collisions, Nucl. Instrum. Methods Phys. Res., Sect. B **262**, 33 (2007).

[19] B. W. Ding, D. Y. Yu, and X. M. Chen, Cross sections for transfer ionization in ion-helium collisions, Nucl. Instrum. Methods Phys. Res., Sect. B **266**, 886 (2008).

[20] B. Ding, H. Li, and W. Zhang, Electron loss accompanied by target ionization for He^+ and Li^{2+} on H and He in low- to intermediate-energy regime, Int. J. Mass Spectrom. **313**, 41 (2012).

[21] D. L. Guo, X. Ma, R. T. Zhang, S. F. Zhang, X. L. Zhu, W. T. Feng, Y. Gao, B. Hai, M. Zhang, H. B. Wang, and Z. K. Huang,

State-selective electron capture in 30- and 100-keV $He^+ + He$ collisions, Phys. Rev. A **95**, 012707 (2017).

[22] C. C. Montanari, J. E. Miraglia, and N. R. Arista, Antiscreening mode of projectile-electron loss, Phys. Rev. A **67**, 062702 (2003).

[23] G. M. Sigaud and E. C. Montenegro, Two-center electron-electron correlation within the independent event model, Braz. J. Phys. **33**, 382 (2003).

[24] I. Mančev, Single-electron capture by hydrogen atoms and helium ions from helium atoms, Phys. Rev. A **54**, 423 (1996).

[25] J. Bradley, S. F. C. O'Rourke, and D. S. F. Crothers, Total and single differential cross sections for simple resonant collisions using a fully orthonormal continuum-distorted-wave basis, Phys. Rev. A **71**, 032706 (2005).

[26] I. Mančev, Four-body continuum-distorted-wave model for charge exchange between hydrogenlike projectiles and atoms, Phys. Rev. A **75**, 052716 (2007).

[27] J. E. Miraglia and M. S. Gravielle, Ionization of He, Ne, Ar, Kr, and Xe by impact of He^+ ions, Phys. Rev. A **81**, 042709 (2010).

[28] N. V. Novikov, Y. A. Teplova, and V. S. Cherhysh, Cross section for the single-electron capture by fast He^+ ions in inert gases, Nucl. Instrum. Methods Phys. Res., Sect. B **269**, 834 (2011).

[29] E. Ghanbari-Adivi and H. Ghavaminia, Single-electron capture from helium atoms by fast singly positive charged helium ions, Eur. Phys. J. D **66**, 1 (2012).

[30] E. Ghanbari-Adivi and H. Ghavaminia, Projectile angular-differential cross sections for single electron transfer in fast He^+-He collisions, Chin. Phys. B **24**, 033401 (2015).

[31] E. Runge and E. K. U. Gross, Density-Functional Theory for Time-Dependent Systems, Phys. Rev. Lett. **52**, 997 (1984).

[32] R. T. Sharp and G. K. Horton, A variational approach to the unipotential many-electron problem, Phys. Rev. **90**, 317 (1953).

[33] J. D. Talman and W. F. Shadwick, Optimized effective atomic central potential, Phys. Rev. A **14**, 36 (1976).

[34] C. A. Ullrich, U. J. Gossmann, and E. K. U. Gross, Time-Dependent Optimized Effective Potential, Phys. Rev. Lett. **74**, 872 (1995).

[35] J. B. Krieger, Y. Li, and G. J. Iafrate, Construction and application of an accurate local spin-polarized Kohn-Sham potential with integer discontinuity: Exchange-only theory, Phys. Rev. A **45**, 101 (1992).

[36] M. A. L. Marques, A. Castro, and A. Rubio, Assessment of exchange-correlation functionals for the calculation of dynamical properties of small clusters in time-dependent density functional theory, J. Chem. Phys. **115**, 3006 (2001).

[37] S. I. Chu, Recent development of self-interaction-free time-dependent density-functional theory for nonperturbative treatment of atomic and molecular multiphoton processes in intense laser fields, J. Chem. Phys. **123**, 062207 (2005).

[38] E. Engel and R. M. Dreizler, From explicit to implicit density functionals, J. Comput. Chem. **20**, 31 (1999).

[39] M. Zapukhlyak, T. Kirchner, H. J. Lüdde, S. Knoop, R. Morgenstern, and R. Hoekstra, Inner- and outer-shell electron dynamics in proton collisions with sodium atoms, J. Phys. B **38**, 2353 (2005).

[40] E. Engel, A. Höck, and R. M. Dreizler, Accuracy of the Krieger-Li-Iafrate approximation for molecules, Phys. Rev. A **62**, 042502 (2000).

[41] M. Keim, A. Werner, D. Hasselkamp, K.-H. Schartner, H. J. Lüdde, A. Achenbach, and T. Kirchner, Lyman-α line polarization after proton impact on atomic hydrogen, J. Phys. B **38**, 4045 (2005).

[42] T. Kirchner, H. J. Lüdde, and M. Horbatsch, A time-dependent quantal approach to electronic transitions in atomic collisions, Recent Res. Dev. Phys. **5**, 433 (2004).

[43] M. Baxter and T. Kirchner, Time-dependent density-functional-theory studies of collisions involving He atoms: Extension of an adiabatic correlation-integral model, Phys. Rev. A **93**, 012502 (2016).

[44] H. J. Lüdde and R. M. Dreizler, Comment on inclusive cross sections, J. Phys. B **18**, 107 (1985).

[45] T. Kirchner, A. C. F. Santos, H. Luna, M. M. Sant'Anna, W. S. Melo, G. M. Sigaud, and E. C. Montenegro, Charge-state-correlated cross sections for electron loss, capture, and ionization in C^{3+}-Ne collisions, Phys. Rev. A **72**, 012707 (2005).

[46] M. Murakami, T. Kirchner, M. Horbatsch, and H. J. Lüdde, Single and multiple electron removal processes in proton–water-molecule collisions, Phys. Rev. A **85**, 052704 (2012).

[47] G. Schenk and T. Kirchner, Multiple ionization of neon atoms in collisions with bare and dressed ions: A mean-field description considering target response, Phys. Rev. A **91**, 052712 (2015).

[48] T. Kirchner and H. Knudsen, Current status of antiproton impact ionization of atoms and molecules: Theoretical and experimental perspectives, J. Phys. B **44**, 122001 (2011).

[49] C. A. Hall and W. W. Meyer, Optimal error bounds for cubic spline interpolation, J. Approximation Theory **16**, 105 (1976).

[50] F. Wilken and D. Bauer, Adiabatic Approximation of the Correlation Function in the Density-Functional Treatment of Ionization Processes, Phys. Rev. Lett. **97**, 203001 (2006).